

Site Symmetry and Multiorbital Flat Bands on Kagome and Pyrochlore Lattices

Keyu Zeng¹ and Ziqiang Wang^{1,*}

¹*Department of Physics, Boston College, Chestnut Hill Massachusetts 02467, USA*

(Dated: March 18, 2024)

Flat bands in electronic band structures are intriguing platforms for strong correlation and topological physics, primarily due to the suppressed kinetic energy of electrons. Various methods have been developed to create flat bands, utilizing lattice geometry or finely tuned parameters. Despite this, the investigation of orbital symmetry in multiorbital materials is a relatively new area of focus. In this work, we propose a site symmetry based systematic approach to emerging multiorbital flat bands in lattices made of corner-connecting motifs such as the kagome and pyrochlore lattices. As a conceptual advance, the one-orbital flat bands are shown to originate as mutual eigenstates of isolated molecular motifs. Further developing the mutual eigenstate method for multiorbitals transforming differently under the site symmetries such as mirror and inversion, we derive multiorbital flat bands from the skew-symmetric interorbital Hamiltonian and introduce an isolated molecule enabled group-theoretic description of the flat band wavefunctions. Realizations of the multiorbital flat bands in relevant materials are shown to be possible under the Slater-Koster formalism. Our findings provide new directions for exploring flat band electronic structures for novel correlated and topological quantum states.

I. INTRODUCTION

The search, discovery, and design of flat bands in electronic structure has attracted much interest due to the potential for realizing novel correlated and topological states of matter such as the fractional quantum anomalous hall state¹⁻⁵. The suppression of kinetic energy allows electron correlation effects to become dominant. An increasing number of theoretical methods have been developed to understand and construct flat bands⁶⁻⁸, including the line-graph method⁹⁻¹² and the compact localized states (CLSs) method¹³⁻¹⁶. Fine-tuning parameters in certain systems can also result in a flat band¹⁷⁻²⁰.

The use of orbital symmetry is a recent advancement in the construction of flat bands.²¹⁻²³ The generic multi-orbital nature of quantum materials makes this a particularly important direction. In this work, we developed a systematic approach to construct multi-orbital flat bands in the 2D kagome and 3D pyrochlore lattices with corner-sharing motifs. We discover that the local site symmetry, such as mirror and inversion, plays a vital role. Inversion even/odd orbitals give rise to singular flat bands with band-touching points, while mirror even/odd orbitals lead to a new type of non-singular flat band in lattices with an odd-number of sublattice sites including the kagome lattice. The origin of the flat bands is the formation of antisymmetric (or skew-symmetric) off-diagonal matrices for the interorbital hopping Hamiltonian. We develop a mutual eigenstate method (MEM) using the isolated molecular approach^{24,25}, for obtaining the flat band wavefunction, and reveal its important correlation with the hopping symmetries necessary for flat band generation. The realization and the topological properties of the site mirror-symmetry generated flat bands are studied for multiorbital materials on the kagome lattice using the Slater-Koster formalism²⁶. The connections to recent experimental findings in the kagome and pyrochlore materials will be discussed.

II. ONE-ORBITAL MODEL AND MEM

The one-orbital tight-binding Hamiltonian with hopping t on the kagome lattice can be written as $H = t \cdot H^K + \mu I$ in the 3-sublattice basis, and

$$H^K = 2 \begin{bmatrix} 0 & \mathbf{c}(\mathbf{k} \cdot \mathbf{r}_{21}) & \mathbf{c}(\mathbf{k} \cdot \mathbf{r}_{31}) \\ \mathbf{c}(\mathbf{k} \cdot \mathbf{r}_{12}) & 0 & \mathbf{c}(\mathbf{k} \cdot \mathbf{r}_{32}) \\ \mathbf{c}(\mathbf{k} \cdot \mathbf{r}_{13}) & \mathbf{c}(\mathbf{k} \cdot \mathbf{r}_{23}) & 0 \end{bmatrix} \quad (1)$$

where μ is the chemical potential, \mathbf{r}_{ij} denotes the hopping vector connecting the sublattice sites i and j in an up triangle in Fig. 1(a), and the wavevector \mathbf{k} is defined in the first Brillouin zone in Fig. 2(b). For brevity, $\mathbf{c}(x) \equiv \cos(x)$ and $\mathbf{s}(x) \equiv \sin(x)$ are used throughout. It is widely known that the band structure obtained from the eigenstates of Eq. (1) contains a flat band, as shown in Fig 1(c). Various methods, including CLSs based on Wannier functions¹² and line-graph of honeycomb lattice²⁷, have been employed to understand the physical and mathematical origin of the flat band.

Since the kagome lattice is made of alternating corner-sharing up and down triangles, the Hamiltonian H^K in Eq. (1) can be decomposed as $H^K = H^\Delta + H^\nabla$,

$$H^{\Delta/\nabla} = \begin{bmatrix} 0 & e^{\mp ik_3} & e^{\pm ik_2} \\ e^{\pm ik_3} & 0 & e^{\mp ik_1} \\ e^{\mp ik_2} & e^{\pm ik_1} & 0 \end{bmatrix}, \quad (2)$$

where $k_i = \epsilon_{ijl} \mathbf{k} \cdot \mathbf{r}_{ij}$. $H^\Delta = (H^\nabla)^*$ is a result of the inversion symmetry at the shared site. We are thus motivated to develop a systematic molecular approach^{24,25} to the flat band states from the localized states on the isolated motifs. The eigenvalues of $H^{\Delta/\nabla}$ are independent of the reciprocal vector \mathbf{k} with n^2 accidental degeneracy at each energy: $E_1 = 2$ in the \mathbb{A}_1 irreducible representation (irrep) and $E_{2/3} = -1$ (irrep \mathbb{E}), corresponding to n^2 isolated triangle molecules. Combining the two non-commuting H^Δ and H^∇ , a flat band arises as a solution

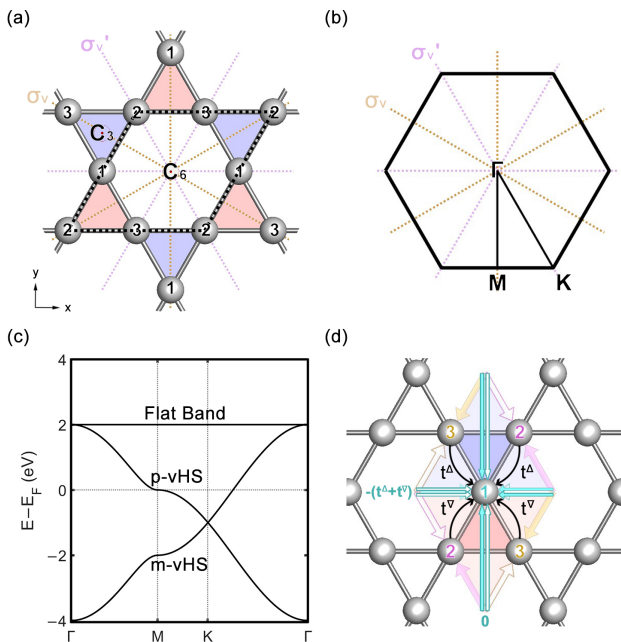


FIG. 1. (a) We use the C_{6v} point group for the 2D kagome lattice and C_{2v} group for the local site symmetry at Wyckoff position $3c$. There are two sets of mirror planes perpendicular to the kagome lattice. The dash lines indicate the unit-cell. (b) Brillouin Zone and high symmetry path of the kagome lattice. (c) Kagome one-orbital band structure with $t = -1.0$. (d) Illustration of mutual eigenstate shared by up and down triangles for one orbital and inversion even and odd interorbital flat bands. The straight arrows (filled: +1; empty: -1) indicate Fourier transformed vectors $\mathbf{r}_{1/2/3} - \mathbf{r}^0$ (three sublattices marked by cyan, magenta and yellow, respectively). The curved black arrows indicate the hopping terms with hopping parameters $t^{\nabla/\Delta}$. The schematic shows that the flat band eigenstate has a \mathbf{k} -independent eigenvalue $-(t^\nabla + t^\Delta)$ and is shared by pink and blue (up/down) triangles.

of the total Hamiltonian H^K when there exists a mutual eigenstate $H^{\Delta/\nabla}|\Psi_{MEM}\rangle = E^{\Delta/\nabla}|\Psi_{MEM}\rangle$. The resulting \mathbf{k} -independent total energy $E_{FB} = E_{MEM}^\Delta + E_{MEM}^\nabla$.

The energy and wavefunction of the flat band can be directly derived from the C_{3v} symmetry of the triangles combined with the C_{2v} site symmetry. The detailed analysis is given in Method. For example, the wavefunction can be constructed using group theory and understood as a linear combination of the degenerate eigenstates in the \mathbb{E} irrep $\Psi_{2/3}^\mathbb{E}$. The flat band solution requires the two-sublattice eigenvector $|\Psi_{3a}\rangle = [1, -1, 0]/\sqrt{2}$ as part of the mutual eigenstate while the orthogonal eigenvector $|\Psi_2\rangle = [-1, -1, 2]/\sqrt{6}$ becomes dispersive. The two degenerate states can be linearly combined into $|\Psi_{3b}\rangle = [-1, 0, 1]/\sqrt{2}$ and $|\Psi_{3c}\rangle = [0, 1, -1]/\sqrt{2}$, forming a C_3 rotation symmetric two-sublattice eigenvector set. The $|\Psi_{3a/b/c}\rangle$ are Fourier transformed with respect to three origins at the center of the adjacent hexagons as shown in Fig. 1(d), and linearly combined in 1 : 1 : 1 ratio to get the final wavefunction $|\Psi_{MEM}\rangle$. At Γ point, $|\Psi_{MEM}\rangle$

vanishes and the degeneracy in \mathbb{E} is recovered by $|\Psi_{2/3}\rangle$. For a general \mathbf{k} point except Γ , the wavefunction is a basis function of the \mathbb{B}_1 irrep of the local site symmetry C_{2v} with $n_{\mathbf{k}}^2 - 1$ accidental degeneracy, which originates from the \mathbb{E}_2 irrep in the induced representation $\text{Ind}(\mathbb{E})_{C_{6v}} = \mathbb{E}_1 + \mathbb{E}_2$ of the point group C_{6v} . The detailed analysis provided in Method leads to

$$E_{FB} = E_{MEM}^\Delta + E_{MEM}^\nabla = -2 \quad (3)$$

$$|\Psi_K^{FB}\rangle = |\Psi_{MEM}\rangle = [\mathbf{s}(k_1), \mathbf{s}(k_2), \mathbf{s}(k_3)]/N. \quad (4)$$

where N is the normalization factor. The odd parity of $|\Psi_K^{FB}\rangle$ is a result of the alternating sign of the two-sublattice wavefunction $|\Psi_{3a/b/c}\rangle$. The single-branch flat band with a double degeneracy touching point at Γ in a one-orbital tight binding model for the kagome lattice is thus explained.

III. INVERSION INTERORBITAL FLAT BAND

We next extend the molecular MEM to construct interorbital flat bands for systems involving two orbitals. Properly orienting the orbitals based on kagome lattice symmetries, the diagonal blocks of the Hamiltonian for intraorbital hopping have the same form as H^K , with orbital-dependent hopping parameters $t_{1/2}$. The off-diagonal interorbital hopping blocks are dependent on the site symmetry of the orbitals. If the two orbitals belong to the same irrep in the site symmetry group, the interorbital hopping will be of the same form as H^K . In this case, absent of intraorbital hopping, the off-diagonal blocks generate two (a bonding and an anti-bonding) sets of typical kagome band dispersions with an effective interorbital hopping $t^\pm = \pm t_{12}$. The flat bands have identical properties with the one-orbital kagome flat band.

New phenomena arise when the two orbitals $O_{1/2}$ transform differently (even or odd) under certain symmetry operations S and thus belong to different irreps $\gamma_{1/2}$ of the site symmetry group: $\chi^{\gamma_{1/2}}(S) = \pm 1$. It is important to note that although the even and odd orbitals belong to different irreps of the local site symmetry, mixing between the orbitals are no longer forbidden at general \mathbf{k} -points in the 2D Brillouin zone because of the lowering of symmetry²⁶. We first consider the case where S corresponds to the inversion operation. Inversion even and odd orbitals have been studied on the square lattice²¹ but with more hoppings beyond the nearest neighbor and parameter tuning. In lattices made of corner-sharing motifs, an exact flat band solution can be achieved. To satisfy the inversion symmetries, the off-diagonal interorbital hopping blocks of the two-orbital Hamiltonian must be antisymmetric (skew-symmetric):

$$H_{6 \times 6}^{oe} = \begin{bmatrix} t_{11}H_{11}^K & t_{12}H_{12}^{AS\dagger} \\ t_{12}H_{12}^{AS} & t_{22}H_{22}^K \end{bmatrix}, \quad (5)$$

where

$$H_{12}^{AS} \equiv H_I^{AS} = 2i \begin{bmatrix} 0 & -\mathbf{s}(k_3) & \mathbf{s}(k_2) \\ \mathbf{s}(k_3) & 0 & -\mathbf{s}(k_1) \\ -\mathbf{s}(k_2) & \mathbf{s}(k_1) & 0 \end{bmatrix}. \quad (6)$$

Mathematically, all odd dimension antisymmetric matrices must have at least one zero eigenvalue because their determinants are zero. That this happens at all \mathbf{k} gives rise to flat bands at zero-energy. The antisymmetric interorbital H_I^{AS} can also be divided into up and down triangles: $H_I^{AS} = H_I^\Delta + H_I^\nabla$. Because the triangles are related by inversion, $H_I^\Delta = H^\Delta - H^\nabla$, which is equivalent to flipping the sign of hopping t_{12} for one set of triangles. Thus, the mutual eigenvector $|\Psi_{MEM}\rangle$ in Eq. (4) for the one-orbital Hamiltonian is also shared by the up and down triangles for H_I^{AS} as illustrated in Fig. 1(d), leading to two degenerate flat bands at energy

$$E_I^{FB} = E_{MEM}^\Delta - E_{MEM}^\nabla = 0, \quad (7)$$

described by flat band wavefunctions

$$\begin{aligned} |\Psi_{O_1}^{FB,I}\rangle &= [\mathbf{s}(k_1), \mathbf{s}(k_2), \mathbf{s}(k_3), 0, 0, 0] / N_0, \\ |\Psi_{O_2}^{FB,I}\rangle &= [0, 0, 0, \mathbf{s}(k_1), \mathbf{s}(k_2), \mathbf{s}(k_3)] / N_0. \end{aligned} \quad (8)$$

The flat bands with band-touching singularity are shown in the two-orbital band dispersion in Fig. 2(a). Note that the odd-parity interorbital flat band wavefunctions in Eq. (8) are also mutual eigenstates of the single-orbital flat band in each orbital sector given in Eq. (4). Consequently, two nondegenerate and perfectly flat bands remain robust even in the presence of significant intraorbital hopping, as shown in Fig. 2(c). The singularity of the flat band at Γ point evolves from Dirac-like under predominant interorbital hopping (Fig. 2a) to quadratic band touching when intraorbital hopping becomes significant (Fig. 2c). Moreover, different inversion symmetries usually involve orbitals of different angular momentum such as the p and d orbitals. The different atomic energies and crystal fields can further separate the singular flat bands of with these unique signatures in realistic materials of kagome as well as pyrochlore materials to be discussed below.

IV. MIRROR INTERORBITAL FLAT BAND

Next, we study the case where the site symmetry S is with respect to all mirror operations and construct the multi-orbital flat bands. Consider a mirror-even orbital and a mirror-odd orbital under S with respect to either set of mirror planes perpendicular to the kagome lattice plane (σ_v and σ'_v). Examples include the p_x and p_y orbitals or the d_{xz} and d_{yz} orbitals described by $\chi_{p_x/d_{xz}}^{B_1}(\sigma_v/\sigma_{v'}) = \pm 1$ and $\chi_{p_y/d_{yz}}^{B_2}(\sigma_v/\sigma_{v'}) = \mp 1$. The resulting interorbital hopping Hamiltonian matrix $H_{12}^{AS} \equiv H_M^{AS}$ must also be antisymmetric, but real and

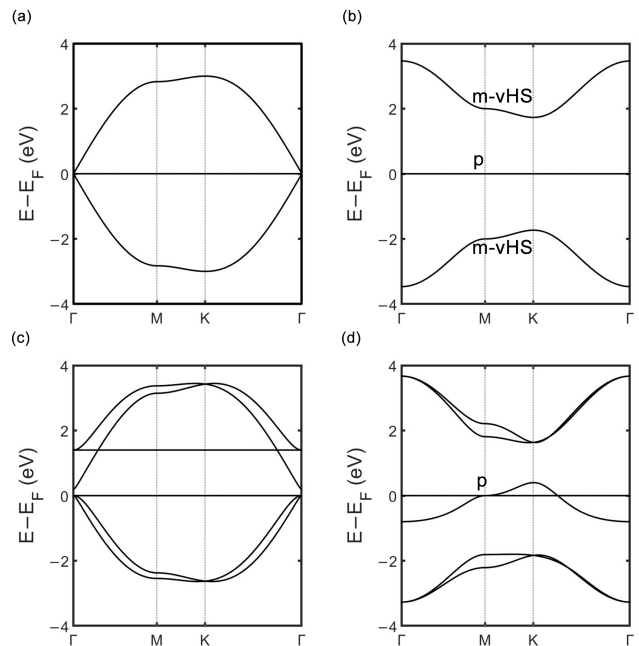


FIG. 2. (a-b) Band dispersion of the two-orbital models showing singular inversion (a) and the nonsingular mirror (b) interorbital flat bands. The interorbital hopping is $t_{12} = 1.0$. Bands are doubly degenerate in the absence of intraorbital hopping. (c-d) Band dispersion in the inversion interorbital model, in the presence of nearest neighbor (nn) intraorbital hopping $t_{11}^{nn} = -0.20$ (c) and the mirror interorbital model, in the presence of nearest neighbor intraorbital hopping $t_{22}^{nn} = 0.20$ (d).

inversion-even:

$$H_M^{AS} = 2 \begin{bmatrix} 0 & -\mathbf{c}(k_3) & \mathbf{c}(k_2) \\ \mathbf{c}(k_3) & 0 & -\mathbf{c}(k_1) \\ -\mathbf{c}(k_2) & \mathbf{c}(k_1) & 0 \end{bmatrix}. \quad (9)$$

The mirror antisymmetric interorbital H_M^{AS} has emergent zero energy flat bands just as the inversion-antisymmetric H_I^{AS} discussed above. Thus, $E_M^{FB} = 0$. There are, however, important differences in their properties. As shown in Fig. 2(b), the mirror antisymmetric flat bands are no longer singular, i.e. without symmetry protected band-touching points with dispersive bands, in contrast to the inversion antisymmetric flat bands shown in Fig. 2(a). The flat band wavefunctions are no longer mutual eigenstates of H^Δ and H^∇ (see below). Moreover, they are different from the flat bands constructed based on chiral operators⁷ since the multi-orbital flat bands in this work do not originate from site number differences but rather from the differences in orbital symmetry.

The flat band wavefunctions can be directly deduced from the lattice harmonics of H_M^{AS} . For a matrix of the form: $H_{3 \times 3}^{AS} = [0, a, -b; -a, 0, c; b, -c, 0]$, its zero-energy eigenvector wavefunction is $|\Psi_0^{AS}\rangle = [c, b, a] / N_0$, where N_0 is a normalization factor. Therefore, in the absence of intraorbital hopping, $|\Psi_0^{AS}\rangle$ is a zero-energy eigenvector

of either orbital of the two-orbital Hamiltonian, leading to the flat band wavefunctions

$$\begin{aligned} |\Psi_{O_1}^{FB,M}\rangle &= [\mathbf{c}(k_1), \mathbf{c}(k_2), \mathbf{c}(k_3), 0, 0, 0] / N_0, \\ |\Psi_{O_2}^{FB,M}\rangle &= [0, 0, 0, \mathbf{c}(k_1), \mathbf{c}(k_2), \mathbf{c}(k_3)] / N_0. \end{aligned} \quad (10)$$

They are parity even under mirror operation. When intraorbital hoppings are added to one of the orbitals, the flatness and pure orbital content of the other orbital's flat band are unchanged, as shown in Figs. 2(d).

The interorbital flat band wavefunction can also be understood using the MEM. The two-orbital Hamiltonian can be divided into four chiral hopping sectors (clockwise: L; counterclockwise: R) on the up/down triangles: $H_M^{oe} = H_R^\Delta + H_L^\Delta + H_R^\nabla + H_L^\nabla$. For the mirror interorbital model, $t_R^\Delta = -t_L^\Delta = t_R^\nabla = -t_L^\nabla = 1$. For each Hamiltonian, there are three degenerate bonding/antibonding eigenstates at energies $E_{B/A} = \pm 1$ described by two-sublattice eigenvectors. A shared eigenvector exists for a combination of inversion-related chiral up and down triangles $H_A = H_R^\Delta + H_L^\nabla$ and $H_B = H_L^\Delta + H_R^\nabla$ with $E_{A/B} = \pm(t^\Delta - t^\nabla) = 0$ and the corresponding wavefunction $|\Psi_{O_i}^{A/B}\rangle = |e^{\pm k_1}, e^{\pm k_2}, e^{\pm k_3}, 0, 0, 0\rangle$ and $|\Psi_{O_2}^{A/B}\rangle = |0, 0, 0, e^{\mp k_1}, e^{\mp k_2}, e^{\mp k_3}\rangle$. It can be shown that $H_A|\Psi_{O_i}^B\rangle = (H_B|\Psi_{O_i}^A\rangle)^*$ is a pure imaginary vector, thus leading to two flat band solutions $|\Psi_{O_i}^{FB,M}\rangle = |\Psi_{O_i}^A\rangle + |\Psi_{O_i}^B\rangle$, as given in Eq. (10), since $(H_A + H_B)|\Psi_{O_i}^{FB,M}\rangle = \mu|\Psi_{O_i}^{FB,M}\rangle$ as the dispersive cross terms cancel out.

It is interesting to note that the mirror interorbital flat band wavefunction $|\Psi_{O_i}^{FB,M}\rangle$ is an even-parity counterpart of the single-orbital kagome flat band wavefunction $|\Psi_K^{FB}\rangle$ in Eq. (4) and the inversion interorbital flat band $|\Psi_{O_i}^{FB,I}\rangle$. Conceptually, the even parity counterpart remains a flat band solution because the hopping sign structure within a triangle motif matches with the one-orbital flat band wavefunction. The difference in the parity of the flat band wavefunctions of the inversion and mirror even/odd Hamiltonians reveals an intriguing mechanism for generating two kinds of flat bands. For singular flat bands with band-touching points to other dispersive bands, such as the ones in the single-orbital and the inversion interorbital band structures shown in Fig. 1(c) and Fig. 2(a), the uniform hopping within the motifs gives rise to mutual eigenstates. By contrast, hopping with alternating signs within each motif breaks the original point group symmetry, but if the signs match with the one-orbital flat band solution, there can be a branch of nonsingular dispersion-canceling eigenstates without band-touching points.

The inversion interorbital flat band can also be understood in a similar way by decomposing the multiorbital Hamiltonian $H_I^{oe} = H_A - H_B$. Because of the minus sign, in order to cancel out $H_A|\Psi_B\rangle + H_B|\Psi_A\rangle$, a flat band wavefunction of $|\Psi_{FB}^I\rangle = |\Psi_A\rangle - |\Psi_B\rangle$ is required, which is the inversion-odd solution (see Method for details) given in Eq. (19). Inversion even/odd orbitals have different orbital angular momentum quantum

number l , while mirror even/odd orbitals can come from the same orbital with different magnetic quantum number m_l or orientations. Thus, on general grounds, large interorbital hoppings between mirror even/odd orbitals are more likely to appear, of which the properties are discussed in the following.

V. PROPERTIES AND REALIZATIONS

The two degenerate flat bands can be shifted in energy by a difference in the crystal field chemical potential μ_1 and μ_2 without disturbing the flatness because they are pure in orbital content. The double-degeneracy of the dispersive bands will be lifted as well. An interesting feature of the mirror or inversion even/odd flat band is a pure site localized wavefunctions at the M point shown in Figs. 2(a-b), which are the same eigenstates as the sublattice polarized p-type van-Hove singularity (vHS) in a single-orbital nn hopping kagome band structure²⁸. In both H^K and H_M^{AS} or H_I^{AS} , the energy of the p-type vHS is pinned by the chemical potentials of the orbitals. With intraorbital nn or second nn hopping added, a H_M^{AS} flat band transforms into a kagome-like dispersion with unchanged p-vHS wavefunctions and energies. This may resolve some unexplained features such as double p-type vHSs in the band structure of real materials²⁹.

To make further connections to realistic materials, we construct explicitly a two-orbital tight-binding Hamiltonian for the d_{xz} and d_{yz} orbitals using the Slater-Koster formalism²⁶. We show that although it is not enforced by the lattice symmetry and affected by intraorbital hopping, the interorbital flat band can play a significant role in the electronic structure of realistic materials. After linear combinations or rotations^{11,30} of the two d -orbitals based on lattice symmetry, we obtain two hybrid orbitals labeled as 1 and 2, as shown in Fig. 3(a), having different mirror symmetry (even and odd) with respect to the mirror planes σ_v or $\sigma_{v'}$. The Hamiltonian $H_{xz/yz}$ has the structure of $H_{6\times 6}^{oe}$ in Eq. (5), where the hopping parameters of the hybrid orbitals determined by the overlap t_δ and t_π for the δ and π bonds: $t_{11} = (t_\pi - 3t_\delta)/2$, $t_{22} = (t_\delta - 3t_\pi)/2$, and $t_{12} = \sqrt{3}(t_\delta + t_\pi)/2$,

$$H_{xz/yz} = \begin{bmatrix} \frac{1}{2}(t_\pi - 3t_\delta)H_{11}^K & \frac{\sqrt{3}}{2}(t_\delta + t_\pi)H_M^{AS\dagger} \\ \frac{\sqrt{3}}{2}(t_\delta + t_\pi)H_M^{AS} & \frac{1}{2}(t_\delta - 3t_\pi)H_{22}^K \end{bmatrix}. \quad (11)$$

As illustrated in Fig. 3(b), the interorbital hopping indeed has an alternating sign structure. Intriguingly, when $t_\pi = 3t_\delta$ or $t_\delta = 3t_\pi$, the intraorbital hopping for one of the hybrid orbitals in the diagonal blocks of Eq. (11) vanishes. Our findings then imply that the associated interorbital flat band would remain perfect flat, while the other becomes significantly dispersive. This is confirmed by the calculated band dispersion plotted in gray lines in Fig. 3(c) and (d), in the presence of a moderate crystal field splitting between the hybrid orbitals “1” and “2”. We thus predict interorbital nearly flat or

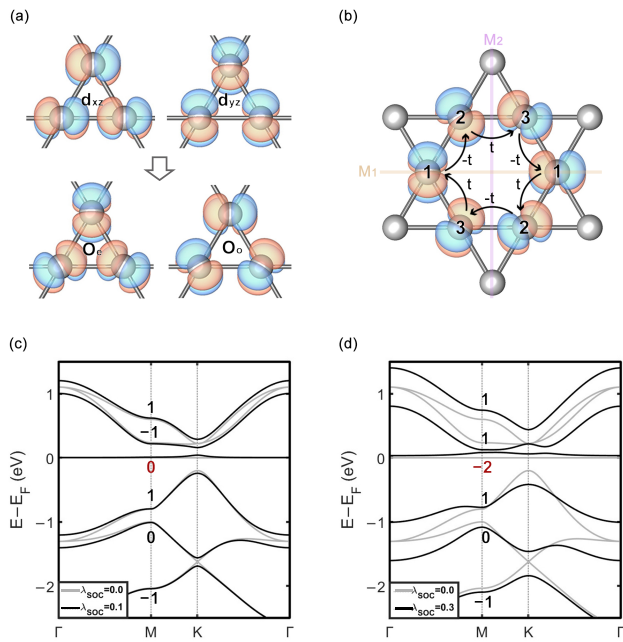


FIG. 3. (a) Linear combination of d_{xz} and d_{yz} orbitals to form two sets of orbital with different mirror symmetry for both sets of mirror planes. (b) Alternating two sets of orbitals on the kagome lattice have alternating signs of inter-orbital hopping parameters. One set of mirror planes that is perpendicular to the kagome lattice is indicated in yellow lines. $t_\pi = 3t_\delta = 0.6$, $\mu_1 = 0.0$, $\mu_2 = -1.0$ for (c) and (d). (c) Flat band disturbed by onsite spin-orbital-coupling with $\lambda_{SOC} = 0.1$, remaining topological trivial when there is no band-crossing. (d) Flat band disturbed by onsite spin-orbital-coupling with $\lambda_{SOC} = 0.3$, becoming topological non-trivial when band-crossing occurs.

narrow bands involving d_{xz} and d_{yz} orbitals in proximity to having $t_\delta : t_\pi = 1 : 3$ or $3 : 1$ in kagome materials.

It is constructive to study the effects of atomic spin-orbit coupling (SOC) $H_{soc} = \lambda_{soc} \mathbf{L} \cdot \mathbf{S}$. Since the hybrid orbitals are $l = 2$ angular momentum eigenstates with magnetic quantum number $m_l = \pm 1$, the SOC leaves the spin component s_z conserved and the up and down spin bands degenerate. For small λ_{soc} , the bands shifts and the band crossings are split as shown in Fig. 3(c). The flat band remains isolated and mostly across the whole Brillouin zone. The calculated Chern number for a single spin projection is marked next to each band, which is the same as the spin Chern number when taking into account the degenerate band of the different spin-projection carrying an opposite Chern number. In this case, the isolated flat band carries zero Chern number. Interestingly, increasing λ_{soc} causes gap between the flat band and the dispersive band to close and reopen as plotted in Fig. 3(d), and endows the flat band with a nontrivial spin-resolved Chern number or a spin Chern number.

Topologically nontrivial flat bands have been investigated for possible realizations of fractionalized anomalous quantum states. When time-reversal symmetry is

broken either spontaneously by correlation effects or by coupling to ferromagnetic structures, partial occupation of the a spin-polarized flat band has the potential for realizing fractional quantum anomalous Hall state or fractional Chern insulators^{1-5,31,32}. When time-reversal symmetry is preserved, partial filling of the degenerate spin-Chern band has the potential of realizing fractional quantum spin Hall state or the proposed fractional topological insulator²¹. The isolated topological multiorbital flat band discussed here can provide a useful direction for material realizations of the fractionalized quantum states.

VI. EXTENSION TO PYROCHLORE

The 3D pyrochlore lattices are made of isolated motif of apex-sharing tetrahedrons with 4-sublattices, as shown in Fig. 4(a). The band dispersions of a single-orbital on the pyrochlore lattice with nearest neighbor hopping are plotted in Fig. 4(c) along the high symmetry directions of the 3D Brillouin zone in Fig. 4(b). Similar to the 2D kagome lattice, the 3D flat band wavefunction in the single-orbital pyrochlore can be understood as the mutual eigenstates of the up (red) and down (blue) tetrahedrons (see Methods). Applying the MEM to the \mathbb{T}_2 irrep of the tetrahedron point group T_d , there are two sets of two-sublattice eigenvectors $\Psi_{j=1,2}^{\mathbb{T}_2}$ that form a shared 3D flat band wavefunction at energy $E_{FB}^P = -2t$,

$$\begin{aligned} |\Psi_a^{FB}\rangle &= [\mathbf{s}(k_{23}), \mathbf{s}(k_{31}), \mathbf{s}(k_{12}), 0] / N_a, \\ |\Psi_b^{FB}\rangle &= [\mathbf{s}(k_{24}), \mathbf{s}(k_{41}), 0, \mathbf{s}(k_{12})] / N_b \end{aligned} \quad (12)$$

where $k_{ij} = \mathbf{k} \cdot (\mathbf{r}_i - \mathbf{r}_j)$. These parity-odd wavefunctions, responsible for the double-degeneracy of the 3D flat bands, are basis functions of the \mathbb{E}_u irrep of the D_{3d} site symmetry.

A natural question is whether 3D interorbital flat bands can be constructed for multiorbital quantum materials on the pyrochlore lattice. Building on the findings on the kagome lattice, we consider two atomic orbitals that even and odd under a site symmetry operation S on the pyrochlore such as $s - p$, $p - d$ or $d - f$ combinations. Because of the four sublattices, the tight-binding Hamiltonian is now an 8×8 matrix of the same form as in Eq. (5). A crucially important difference from the kagome lattice is that the 4×4 off-diagonal antisymmetric interorbital hopping matrix (H_{12}^{AS}) is now even-dimensional. As a result, only inversion even/odd H_I^{AS} is allowed, but mirror even/odd H_M^{AS} vanishes in a two-orbital model due to the impossible sign alternations to satisfy all mirror or C_2 operations. The antisymmetric inversion even/odd interorbital Hamiltonian $H_{12}^{AS} \equiv H_I^{AS}$ on the pyrochlore lattice is given by

$$H_{12} = 2i \begin{bmatrix} 0 & -\mathbf{s}(k_{21}) & -\mathbf{s}(k_{31}) & -\mathbf{s}(k_{41}) \\ \mathbf{s}(k_{12}) & 0 & -\mathbf{s}(k_{32}) & -\mathbf{s}(k_{42}) \\ \mathbf{s}(k_{13}) & \mathbf{s}(k_{23}) & 0 & -\mathbf{s}(k_{43}) \\ \mathbf{s}(k_{14}) & \mathbf{s}(k_{24}) & \mathbf{s}(k_{34}) & 0 \end{bmatrix}. \quad (13)$$

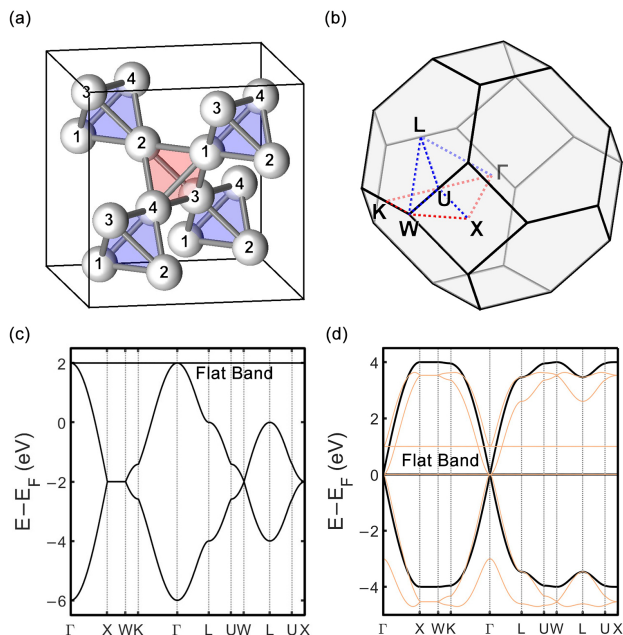


FIG. 4. (a) Pyrochlore lattice structure consisting of up and down tetrahedrons. The solid lines indicate the unit-cell. (b) Brillouin Zone and high symmetry path. (c) Pyrochlore one-orbital band structure with $t = -1.0$, where there are doubly-degenerate flat bands. (d) Inversion interorbital flat band with $t_{12} = 1.0$ and $t_1 = 0.0, t_2 = 0.0$ (black thick line) or $t_1 = -0.5, t_2 = 0.0$ (orange thin line).

Note that the determinant of an even-dimensional anti-symmetric matrix is a Pfaffian, which is usually non-zero. Surprisingly, the inversion interorbital matrix in Eq. (13) has a zero determinant $\text{Det}(H_{12}^{AS}) = 0$. The flat band wavefunctions are given by

$$\begin{aligned} |\Psi_{O_1,a}^{FB}\rangle &= [\mathbf{s}(k_{23}), \mathbf{s}(k_{31}), \mathbf{s}(k_{12}), 0, 0, 0, 0] / N_a, \\ |\Psi_{O_1,b}^{FB}\rangle &= [\mathbf{s}(k_{24}), \mathbf{s}(k_{41}), 0, \mathbf{s}(k_{12}), 0, 0, 0] / N_b, \end{aligned} \quad (14)$$

$$\begin{aligned} |\Psi_{O_2,a}^{FB}\rangle &= [0, 0, 0, 0, \mathbf{s}(k_{23}), \mathbf{s}(k_{31}), \mathbf{s}(k_{12}), 0] / N_a, \\ |\Psi_{O_2,b}^{FB}\rangle &= [0, 0, 0, 0, \mathbf{s}(k_{24}), \mathbf{s}(k_{41}), 0, \mathbf{s}(k_{12})] / N_b. \end{aligned} \quad (15)$$

In the inversion interorbital model, there is a new Dirac crossing at Γ point in both kagome and pyrochlore lattices as shown in Fig. 2(a) and Fig. 4(d). Similar to the kagome lattice, the inversion interorbital flat bands on the pyrochlore lattice have the remarkable property that their flatness is robust against significant intra-orbital hopping, which only causes shifting of the flat band energies, as explicitly shown in Fig. 4(d).

In realistic band structures, a hybrid of quadratic and Dirac crossing may occur. Whether the interorbital hopping is dominant or not can be judged by the features

of the dispersive bands with respect to the singular flat band. For instance, in a recent study³³ of CuV_2S_4 , which contains a pyrochlore structure, the interorbital Dirac crossing features of the dispersive bands dominate over quadratic band touching at Γ point, pointing to the proximity to an inversion interorbital flat band between different atoms (possibly of Cu d and S p orbitals) with significant interorbital hopping.

VII. SUMMARY AND OUTLOOK

We introduced a new theoretical framework to discover and construct singular and nonsingular flat bands in multi-orbital 2D kagome and 3D pyrochlore crystals. These lattice structures have corner-sharing motifs containing either an odd or an even number of sublattices, which are shown to be suitable for the isolated molecular approach and the mutual eigenstate method. We showed that the local site-symmetry S plays a crucial role for the emergence of multi-orbital flat bands and wave functions are found for S corresponding to the local inversion and mirror symmetries on the kagome lattice, and for local inversion on the 3D pyrochlore lattice. Specific atomic realizations of such multi-orbital flat bands are constructed in the Slater-Koster framework and the potential to host novel topological states are studied for the mirror even/odd orbitals on the kagome lattice. The proposed mechanism for the multi-orbital flat bands are directly relevant for the search and design of flat bands in kagome and pyrochlore materials for studying novel correlated and topological quantum states. It may potentially explain the flat band high spectral intensity buildup around the van Hove singularities below the Fermi level observed in kagome metals CsTi_3Bi_5 ³⁴, CsV_3Sb_5 ³⁵, and the pyrochlore metal CuV_2S_4 ³³ materials. The findings in this study may pave the way for new directions in flat band exploration and the understanding of multi-orbital electronic structures.

VIII. ACKNOWLEDGEMENT

We thank Jie Liu and Zhan Wang for valuable discussions. The work is supported by the U.S. Department of Energy, Basic Energy Sciences Grant DE-FG02-99ER45747 and by Research Corporation for Science Advancement Cottrell SEED Award No. 27856.

IX. REFERENCE

* wangzi@bc.edu

¹ T.-H. Han, J. S. Helton, S. Chu, D. G. Nocera, J. A. Rodriguez-Rivera, C. Broholm, and Y. S. Lee, *Nature*

- 492**, **406** (2012), number: 7429 Publisher: Nature Publishing Group.
- ² D. N. Sheng, Z.-C. Gu, K. Sun, and L. Sheng, *Nature Communications* **2**, **389** (2011), number: 1 Publisher: Nature Publishing Group.
 - ³ Y.-F. Wang, Z.-C. Gu, C.-D. Gong, and D. N. Sheng, *Physical Review Letters* **107**, **146803** (2011), publisher: American Physical Society.
 - ⁴ T. Neupert, L. Santos, C. Chamon, and C. Mudry, *Physical Review Letters* **106**, **236804** (2011), publisher: American Physical Society.
 - ⁵ N. Regnault and B. A. Bernevig, *Physical Review X* **1**, **021014** (2011), publisher: American Physical Society.
 - ⁶ D. Leykam, A. Andreanov, and S. Flach, *Advances in Physics: X* **3**, **1473052** (2018).
 - ⁷ D. Călugăru, A. Chew, L. Elcoro, Y. Xu, N. Regnault, Z.-D. Song, and B. A. Bernevig, *Nature Physics* **18**, **185** (2022), number: 2 Publisher: Nature Publishing Group.
 - ⁸ P. M. Neves, J. P. Wakefield, S. Fang, H. Nguyen, L. Ye, and J. G. Checkelsky, “Crystal Net Catalog of Model Flat Band Materials,” (2023), arXiv:2303.02524 [cond-mat].
 - ⁹ C. V. Morfonios, M. Röntgen, M. Pyzh, and P. Schmelcher, *Physical Review B* **104**, **035105** (2021), publisher: American Physical Society.
 - ¹⁰ C. S. Chiu, D.-S. Ma, Z.-D. Song, B. A. Bernevig, and A. A. Houck, *Physical Review Research* **2**, **043414** (2020), publisher: American Physical Society.
 - ¹¹ H. Liu, G. Sethi, S. Meng, and F. Liu, *Physical Review B* **105**, **085128** (2022).
 - ¹² Y. Hwang, J.-W. Rhim, and B.-J. Yang, *Physical Review B* **104**, **085144** (2021), publisher: American Physical Society.
 - ¹³ W. Maimaiti, A. Andreanov, H. C. Park, O. Gendelman, and S. Flach, *Physical Review B* **95**, **115135** (2017), publisher: American Physical Society.
 - ¹⁴ W. Maimaiti, A. Andreanov, and S. Flach, *Physical Review B* **103**, **165116** (2021), publisher: American Physical Society.
 - ¹⁵ W. Maimaiti, S. Flach, and A. Andreanov, *Physical Review B* **99**, **125129** (2019), publisher: American Physical Society.
 - ¹⁶ Y. Chen, J. Huang, K. Jiang, and J. Hu, “Decoding flat bands from compact localized states,” (2022), arXiv:2212.13526 [cond-mat].
 - ¹⁷ T. Mizoguchi and M. Udagawa, *Physical Review B* **99**, **235118** (2019), publisher: American Physical Society.
 - ¹⁸ T. Ogata, M. Kawamura, and T. Ozaki, *Physical Review B* **103**, **205119** (2021).
 - ¹⁹ C.-C. Lee, A. Fleurence, Y. Yamada-Takamura, and T. Ozaki, *Physical Review B* **100**, **045150** (2019), publisher: American Physical Society.
 - ²⁰ T. Misumi and H. Aoki, *Physical Review B* **96**, **155137** (2017), publisher: American Physical Society.
 - ²¹ K. Sun, Z. Gu, H. Katsura, and S. Das Sarma, *Physical Review Letters* **106**, **236803** (2011), publisher: American Physical Society.
 - ²² J. W. F. Venderbos, M. Daghofer, and J. van den Brink, *Physical Review Letters* **107**, **116401** (2011), publisher: American Physical Society.
 - ²³ T. Mizoguchi and Y. Hatsugai, *Physical Review B* **101**, **235125** (2020).
 - ²⁴ T. Mizoguchi, M. Maruyama, S. Okada, and Y. Hatsugai, *Physical Review Materials* **3**, **114201** (2019), publisher: American Physical Society.
 - ²⁵ T. Mizoguchi, H. Katsura, I. Maruyama, and Y. Hatsugai, *Physical Review B* **104**, **035155** (2021), publisher: American Physical Society.
 - ²⁶ J. C. Slater and G. F. Koster, *Physical review* **94**, **1498** (1954), publisher: APS.
 - ²⁷ A. Mielke, *Journal of Physics A: Mathematical and General* **24**, **L73** (1991).
 - ²⁸ M. L. Kiesel and R. Thomale, *Physical Review B* **86**, **121105** (2012).
 - ²⁹ Y. Hu, X. Wu, B. R. Ortiz, S. Ju, X. Han, J. Ma, N. C. Plumb, M. Radovic, R. Thomale, S. D. Wilson, A. P. Schnyder, and M. Shi, *Nature Communications* **13**, **2220** (2022).
 - ³⁰ X. Wu, T. Schwemmer, T. Müller, A. Consiglio, G. Sangiovanni, D. Di Sante, Y. Iqbal, W. Hanke, A. P. Schnyder, M. M. Denner, M. H. Fischer, T. Neupert, and R. Thomale, *Physical Review Letters* **127**, **177001** (2021), publisher: American Physical Society.
 - ³¹ M. Kang, S. Fang, L. Ye, H. Po, J. Denlinger, C. Jozwiak, A. Bostwick, E. Rotenberg, E. Kaxiras, J. Checkelsky, and R. Comin, *Nature Communications* **11** (2020), **10.1038/s41467-020-17465-1**.
 - ³² S. Okamoto, N. Mohanta, E. Dagotto, and D. N. Sheng, *Communications Physics* **5**, **1** (2022), number: 1 Publisher: Nature Publishing Group.
 - ³³ J. Huang, L. Chen, Y. Huang, C. Setty, B. Gao, Y. Shi, Z. Liu, Y. Zhang, T. Yilmaz, E. Vescovo, M. Hashimoto, D. Lu, B. I. Yakobson, P. Dai, J.-H. Chu, Q. Si, and M. Yi, *Nature Physics* , **1** (2024), publisher: Nature Publishing Group.
 - ³⁴ J. Yang, X. Yi, Z. Zhao, Y. Xie, T. Miao, H. Luo, H. Chen, B. Liang, W. Zhu, Y. Ye, J.-Y. You, B. Gu, S. Zhang, F. Zhang, F. Yang, Z. Wang, Q. Peng, H. Mao, G. Liu, Z. Xu, H. Chen, H. Yang, G. Su, H. Gao, L. Zhao, and X. J. Zhou, *Nature Communications* **14**, **4089** (2023).
 - ³⁵ H. Luo, L. Zhao, Z. Zhao, H. Yang, Y.-P. Huang, H. Liu, Y. Gu, F. Jin, H. Chen, T. Miao, C. Yin, C. Shen, X. Ren, B. Liang, Y. Shu, Y. Chen, F. Zhang, F. Yang, S. Zhang, Q. Peng, H. Mao, G. Liu, J. Hu, Y. Shi, Z. Xu, K. Jiang, Q. Zhang, Z. Wang, H. Gao, and X. J. Zhou, “van Hove Singularity-Driven Emergence of Multiple Flat Bands in Kagome Superconductors,” (2024), arXiv:2403.06085.
 - ³⁶ Y. Hwang, J.-W. Rhim, and B.-J. Yang, *Physical Review B* **104**, **L081104** (2021), publisher: American Physical Society.
 - ³⁷ J. P. Wakefield, M. Kang, P. M. Neves, D. Oh, S. Fang, R. McTigue, S. Y. Frank Zhao, T. N. Lamichhane, A. Chen, S. Lee, S. Park, J.-H. Park, C. Jozwiak, A. Bostwick, E. Rotenberg, A. Rajapitamahuni, E. Vescovo, J. L. McChesney, D. Graf, J. C. Palmstrom, T. Suzuki, M. Li, R. Comin, and J. G. Checkelsky, *Nature* **623**, **301** (2023), number: 7986 Publisher: Nature Publishing Group.

X. METHOD

A. General Proof of the Symmetry Structure

The mirror symmetry operator M along the y -direction that keeps site-1 invariant while exchanging site-2 with site-3 can be expressed as a 6×6 matrix in

the two-orbital basis C for the even/odd orbitals:

$$M = \begin{bmatrix} 1 & 0 & 0 & 0 & 0 & 0 \\ 0 & 0 & 1 & 0 & 0 & 0 \\ 0 & 1 & 0 & 0 & 0 & 0 \\ 0 & 0 & 0 & -1 & 0 & 0 \\ 0 & 0 & 0 & 0 & 0 & -1 \\ 0 & 0 & 0 & 0 & -1 & 0 \end{bmatrix}, \quad C = \begin{bmatrix} c_1^e \\ c_2^e \\ c_3^e \\ c_1^o \\ c_2^o \\ c_3^o \end{bmatrix} \quad (16)$$

The other set of mirror symmetries can also be represented in similar ways. The Hamiltonian satisfies: $MHM^{-1} = H$. Therefore, the interorbital hopping has the antisymmetric form: $\epsilon_{ijk} t_{ij} c_i^e c_j^o$, where ϵ_{ijk} is the total antisymmetric tensor.

Another way to describe the symmetry structure is based on the two-center integral approximation²⁶, where the hopping strength is approximated by the atomic orbital overlap $f^{\alpha\beta} = \int \Psi^\alpha \Psi^\beta dr^3$. The representation of the hopping parameters can be determined: $\chi_{f^{\alpha\beta}}^\gamma(S) = \chi_{\Psi^\alpha}^{\gamma\alpha}(S) \chi_{\Psi^\beta}^{\gamma\beta}(S)$, where S is a local site symmetry. For the kagome lattice, $\chi_{f^{\alpha\beta}}^\gamma(S)$ are all one-dimensional irreps and the intraorbital hopping for any orbital gives $\chi_{f^{\alpha\beta}}^\gamma(S) = 1$ and $\gamma = \mathbb{A}_1$. Therefore, all intraorbital hopping matrix exhibits simple s-orbital symmetry. For the interorbital hopping between, e.g. mirror even and odd orbitals, $\chi_f^\gamma = \chi_{d_{xz}}^{\mathbb{B}_1} \chi_{d_{yz}}^{\mathbb{B}_2}$, $\gamma = \mathbb{B}_1 \otimes \mathbb{B}_2 = \mathbb{A}_2$. Thus, the interorbital hopping terms $t_{ij}^{\alpha\beta} c_i^\alpha c_j^\beta$ should transform under this two-dimensional irrep. For the pyrochlore lattice, the two-dimensional irreps become complicated with complex representations. For example, $\chi_f^\gamma = \chi_{d_{xz}}^{\mathbb{E}_g} \chi_{d_{yz}}^{\mathbb{E}_g} = \mathbb{E}_g \otimes \mathbb{E}_g = \mathbb{A}_{1g} + \mathbb{A}_{2g} + \mathbb{E}_g$.

B. MEM for Single Orbital Model

The eigenvectors of a triangle molecule are: $|\Psi_1\rangle = [1, 1, 1]/\sqrt{3}$, $|\Psi_2\rangle = [-1, -1, 2]/\sqrt{6}$ and $|\Psi_{3a}\rangle = [-1, 1, 0]/\sqrt{2}$. The latter two degenerate states can be linearly combined into $|\Psi_{3b}\rangle = [1, 0, -1]/\sqrt{2}$ and $|\Psi_{3c}\rangle = [0, -1, 1]/\sqrt{2}$, which together with $|\Psi_{3a}\rangle$ form a C_3 rotation symmetric eigenvector set. Placing up (down) triangle molecules on a triangular net with aligned equal triangle edges \mathbf{a}_i and shared vertexes results in the kagome lattice. The eigenvectors of N molecular H^Δ and H^∇ in the kagome lattice is equivalent to a Fourier transform of the molecular eigenvectors based on the translation symmetry of the triangular lattice, while the eigenvalues remain degenerate and independent of \mathbf{k} :

$$\begin{aligned} |\Psi_1^{\Delta/\nabla}\rangle &= [e^{\pm ik_1}, e^{\pm i(k_1 - k_3)}, e^{\pm ik_3}] / N_1, \\ |\Psi_2^{\Delta/\nabla}\rangle &= [-e^{\pm ik_1}, -e^{\pm i(k_1 - k_3)}, 2e^{\pm ik_3}] / N_2, \\ |\Psi_{3a}^{\Delta/\nabla}\rangle &= [-e^{\pm ik_1}, e^{\pm ik_2}, 0] / N_3. \end{aligned}$$

The two sets of eigenvectors form the eigenspaces of the Hamiltonians of the up and down triangles, spanning the

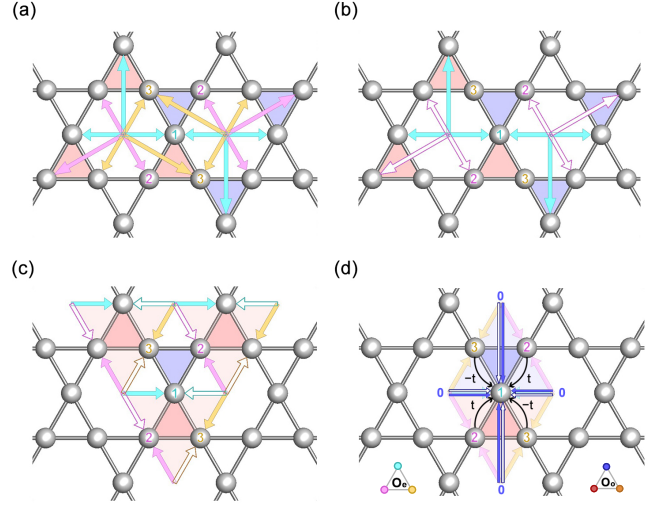


FIG. 5. Up/down triangles are marked in red/blue faces. $|\mathbf{r}_{1/2/3} - \mathbf{r}_{a/b/c}^0|$ belonging to different sublattices 1/2/3 are colored in cyan, magenta and yellow, and $w = \pm 1$ is in filled and empty arrows, respectively. (a) Schematics for $|\Psi_1^\Delta\rangle$ (left) and $|\Psi_1^\nabla\rangle$ (right). (b) Schematics for $|\Psi_{3a/b/c}^\Delta\rangle$ (left) and $|\Psi_{3a/b/c}^\nabla\rangle$ (right) before linear combination. (c) Mutual eigenvector obtained by linear combination $|\Psi_{3a/b/c}^\Delta\rangle$ matches for up and down triangles. (d) Antisymmetric hopping for $|\Psi_{O_1}^{FB,M}\rangle$ from orbital O_1 (light colors) to site 1 orbital O_2 (dark colors).

same \mathbf{k} -space,

$$H^{\Delta/\nabla} = t^{\Delta/\nabla} \begin{bmatrix} 0 & e^{\mp ik_3} & e^{\pm ik_2} \\ e^{\pm ik_3} & 0 & e^{\mp ik_1} \\ e^{\mp ik_2} & e^{\pm ik_1} & 0 \end{bmatrix}. \quad (17)$$

The Hamiltonians and eigenvectors of the up and down triangles are complex conjugate of each other due to the inversion symmetry relating the two sets of triangles. The degeneracy of the energies at $E = -t$ corresponds to the band-touching degenerate point at the Γ point. Away from the Γ point, the degeneracy is lifted and only one eigenvector still has dispersivenessless energy, which is the mutual eigenstate of $H^{\Delta/\nabla}$. To find the shared eigenspace, a linear combination of \mathbf{k} -space eigenvectors with different origins is performed,

$$\begin{aligned} \Phi^{\gamma_j \mathbf{k}} &= \sum_{m=1}^3 \sum_{n=1}^{n_o} \sum_{i=1}^{d_j} e^{i\mathbf{k} \cdot (\mathbf{r}_m - \mathbf{r}_n^0)} a_i w_{i,m}^{\gamma_j} c_{\mathbf{k},m}^\dagger \\ &= \sum_{n=1}^{n_o} \sum_{i=1}^{d_j} a_i \Psi_i^{\gamma_j}(\mathbf{k}, n) \end{aligned} \quad (18)$$

which is allowed by the energy degeneracy for all \mathbf{k} -point. Here a_i is the linear combination coefficients between different eigenstates, $w_{i,m}^{\gamma_j}$ is the eigenstate coefficients for m -th site in the i -th eigenvector of irrep γ_j , and $\{\mathbf{r}_n^0\}$ is a limited set of $n_o \ll N$ origins.

The mutual eigenvector satisfies invariance under inversion: $g_I \Phi_k^{\gamma_j} = \pm \Phi_{g_I k}^{\gamma_j}$, each site remains themselves under inversion thus a set of inversion related $g_I(\mathbf{r}_m - \mathbf{r}_n^0) = \mathbf{r}_m - \mathbf{r}_n^0$ becomes the main requirement as shown in Fig 5(c). By contrast, before linear combination, the $|\Psi_{1/2/3}^\Delta\rangle$ does not match with the right eigenvector $|\Psi_{1/2/3}^\nabla\rangle$ pattern because they are not inversion invariant as shown in Fig 5(a) and (b). The problem is thus transformed into finding a proper set of origins and eigenvectors.

For an origin \mathbf{r}_n^0 , if there exists $|\mathbf{r}_p - \mathbf{r}_n^0| \neq |\mathbf{r}_q - \mathbf{r}_n^0|$ for non-zero $w_{i,p/q}^{\gamma_j}$ (number of w can be two or three), there must exist another origin \mathbf{r}_n^0 in order to form the inversion pair for site p or q . Because there is no possibility for a one-sublattice eigenstate in \mathbb{E} , if $|\mathbf{r}_p - \mathbf{r}_n^0| = |\mathbf{r}_p - \mathbf{r}_n^0|$, there must exist $|\mathbf{r}_s - \mathbf{r}_n^0| \neq |\mathbf{r}_p - \mathbf{r}_n^0| \neq |\mathbf{r}_s - \mathbf{r}_n^0|$. As a consequence, the number of origins quickly increase $n_o \rightarrow Z * N$, where $Z \leq D(C_{6v})$ and won't enclose. In a word, $\{\mathbf{r}_m - \mathbf{r}_n^0\} (m = |w_{i,p/q}^{\gamma_j}| \neq 0)$ is not inversion invariant unless for any non-zero $w_{i,p/q}^{\gamma_j}$, $|\mathbf{r}_p - \mathbf{r}_n^0| = |\mathbf{r}_q - \mathbf{r}_n^0|$. The center of the triangles can also be excluded from the origin choice due to the infinite propagation of the inversion-pair vectors. As a result, only the eigenvectors $|\Psi_{3a/b/c}\rangle$ with two non-zero $w_{i,p/q}^{\gamma_j}$ (two-sublattice for short) satisfy the above requirement. Meanwhile the origins and their inversion partners have to lie on the three mirror planes σ_v bisecting the bonds to satisfy the conditions simultaneously, which are the center of the hexagons. Around one triangle, there are three hexagon centers, forming a set of $\{|\mathbf{r}_m - \mathbf{r}_n^0|\}$ that contains all point group symmetry partners $g_I |\mathbf{r}_m - \mathbf{r}_n^0|$.

Thus we have derived the flat band solution $|\Psi_K^{FB}\rangle$. Because the eigenvectors $|\Psi_{3a/b/c}\rangle$ are odd with respect to the mirror planes bisecting corresponding bonds, the combined eigenvector $|\Psi_K^{FB}\rangle$ is odd with respect to inversion symmetry as shown in Fig. 5: $|\Psi_K^{FB}\rangle = [\mathbf{s}(k_1), \mathbf{s}(k_2), \mathbf{s}(k_3)]/N$. The description of \mathbb{B}_1 irrep is for the wavefunction under the site symmetry C_{2v} . The resulting wavefunction is the shared eigenstate of H^Δ and H^∇ and has a k -independent total energy $E_K^{FB} = E_3^\Delta + E_3^\nabla = -t^\Delta - t^\nabla = -2t$ for the one-orbital model, and $-t - (-t) = 0$ for the inversion even/odd interorbital model.

This process for more than two sublattices necessitates the linear combination of degenerate eigenvectors, leading to an inevitable band touching between the resulting flat band and other dispersive bands, as mandated by symmetry³⁶. Similarly, the flat bands in the pyrochlore structure also touch other dispersive bands at Γ point³⁷. The wavefunction can also be constructed using the two-sublattice eigenvectors ($E_{T_2} = -t$) with $w_p^{T_2} = 1, w_q^{T_2} = -1, w_r^{T_2} = w_s^{T_2} = 0$ in the three-fold degenerate irrep T_2 for a tetrahedron belonging to the T_d group. Combined with the site symmetry D_{3d} , there are two sets of two-sublattice solutions out of the three degenerate eigenstates with $E_{1/2/3}^P = -t$:

$|\Psi_1^P\rangle = [1, 1, -1, -1]/2$, $|\Psi_2^P\rangle = [1, -1, 0, 0]/\sqrt{2}$, and $|\Psi_3^P\rangle = [0, 0, 1, -1]/\sqrt{2}$. They form the two degenerate flat bands solution belonging to the site symmetry irrep \mathbb{E}_u with energy $E_{FB}^P = E_{T_2}^\Delta + E_{T_2}^\nabla = -t^\Delta - t^\nabla = -2t$ for the one-orbital model, and $-t - (-t) = 0$ for the inversion even/odd interorbital model.

C. MEM for Two Orbital Model

In the one-orbital model, the hopping term $tf(\mathbf{k})_{ij}c_i^\dagger(\mathbf{k})c_j(\mathbf{k}) = (tf(\mathbf{k})_{ji}c_j^\dagger(\mathbf{k})c_i(\mathbf{k}))^\dagger$. Thus, there is no extra degrees of freedom to further divide H^Δ and H^∇ . By contrast, in the two-orbital model, because of the possible orbital combinations $H^{\Delta/\nabla}$ can be further divided into left and right handed chiral hopping channels. For example, the right-handed interorbital chiral hoppings are defined according to $c_{O1,j}^\dagger(\mathbf{k})c_{O2,i}(\mathbf{k})$ with $\{ij\} = \{12\}, \{23\}, \{31\}$. As a result, the mirror even/odd interorbital Hamiltonian is decomposed as

$$H_M^{oe} = H_R^\Delta + H_L^\Delta + H_R^\nabla + H_L^\nabla,$$

where

$$H_R^{\Delta/\nabla} = t_R^{\Delta/\nabla} \begin{bmatrix} 0 & 0 & 0 & 0 & e^{\mp ik_3} & 0 \\ 0 & 0 & 0 & 0 & 0 & e^{\mp ik_1} \\ 0 & 0 & 0 & e^{\mp ik_2} & 0 & 0 \\ 0 & 0 & e^{\pm ik_2} & 0 & 0 & 0 \\ e^{\pm ik_3} & 0 & 0 & 0 & 0 & 0 \\ 0 & e^{\pm ik_1} & 0 & 0 & 0 & 0 \end{bmatrix}$$

and

$$H_L^{\Delta/\nabla} = t_L^{\Delta/\nabla} \begin{bmatrix} 0 & 0 & 0 & 0 & 0 & e^{\pm ik_2} \\ 0 & 0 & 0 & e^{\pm ik_3} & 0 & 0 \\ 0 & 0 & 0 & 0 & e^{\pm ik_1} & 0 \\ 0 & e^{\mp ik_3} & 0 & 0 & 0 & 0 \\ 0 & 0 & e^{\mp ik_1} & 0 & 0 & 0 \\ e^{\mp ik_2} & 0 & 0 & 0 & 0 & 0 \end{bmatrix}$$

Here, $t_R^\Delta = -t_L^\nabla = t$ and $t_R^\nabla = -t_L^\Delta = t$ are required to construct the antisymmetric interorbital Hamiltonian H_{12} . The eigenstates for these chiral hopping Hamiltonians around the up and down triangles are the interorbital bonding/antibonding states on the three bonds. They are therefore triple-degenerate two-sublattice wavefunctions. As a result, the constructed mutual eigenstates for $H_A = H_R^\Delta + H_L^\nabla$ and $H_B = H_L^\Delta + H_R^\nabla$ are: $|\Psi_{A/B}^1\rangle = [e^{\pm ik_1}, e^{\pm ik_2}, e^{\pm ik_3}, e^{\mp ik_1}, e^{\mp ik_2}, e^{\mp ik_3}]/N_1$, $|\Psi_{A/B}^2\rangle = [-e^{\pm ik_1}, -e^{\pm ik_2}, -e^{\pm ik_3}, e^{\mp ik_1}, e^{\mp ik_2}, e^{\mp ik_3}]/N_1$. These states form flat bands at zero energy, which is a result of the hopping with opposite sign on the up and down triangles. $|\Psi_{A/B}^i\rangle$ can be linearly combined into orbital pure wavefunctions, which will be the eigenstates for when the chemical potential and crystal fields $\mu_{O1} \neq \mu_{O2} \neq 0$.

Next to find the total eigenstate for $H_M^{oe} = H_A + H_B$ or $H_I^{oe} = H_A - H_B$, we calculate the cross

terms $H_A|\Psi_B\rangle$ and $H_B|\Psi_A\rangle$ and obtain $H_A|\Psi_B\rangle = it[\mathbf{s}(k_2 - k_3), \mathbf{s}(k_3 - k_1), \mathbf{s}(k_1 - k_2), 0, 0, 0]/N$, which is purely imaginary, and $H_A|\Psi_B\rangle = (H_B|\Psi_A\rangle)^*$. As a consequence, $H_A|\Psi_B\rangle + H_B|\Psi_A\rangle = \text{Real}(H_A|\Psi_B\rangle) = 0$. Therefore, for the total eigenstate to remain a flat band solution, the parity of the wavefunction should match with the total Hamiltonian:

$$\begin{aligned} & (H_A \pm H_B)(|\Psi_A\rangle \pm |\Psi_B\rangle) \\ &= \mu(|\Psi_A\rangle + |\Psi_B\rangle) \pm (H_A|\Psi_B\rangle + H_B|\Psi_A\rangle) \\ &= \mu(|\Psi_A\rangle + |\Psi_B\rangle) \end{aligned} \quad (19)$$

D. Definition of Up and Down Tetrahedrons

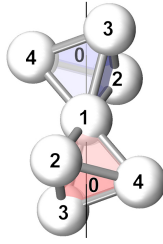


FIG. 6. Up (red) and down (blue) tetrahedrons.

The tetrahedron is defined in the following way: form a perpendicular line \mathbf{r}_{10} from site-1 to the center of triangle of site-2/3/4. Up tetrahedron is a right-handed triangle 234 around the axis \mathbf{r}_{10} , and down tetrahedron is a left-handed triangle 234 around the axis \mathbf{r}_{10} .